COMMUNICATION

Check for updates

Laser engineering of heterostructured graphitic petals on carbon nanotube forests for robust thermal interface capable of swift heat transfer†

Prashant Kumar, [ID] *[abc] Qiong Nian, [ID] ‡[ab] Guoping Xiong, [ID] §[ad] Timothy S. Fisher¶[ad] and Gary J. Cheng [ID] *[abd]

Amongst graphene-carbon nanotube hybrid-based thermal interfaces, graphene petals (GP) grown on CNT forests (CNTF) seem apt, but petals grown out-of-plane gives compromised heat transfer when integrated to a heat sink. To address these technological challenges, KrF (248 nm) laser annealing and Nd-YAG laser shock peening of microwave plasma chemical vapour deposition (MPCVD) grown GP/CNTF have been employed for the first time and the discovery is reported here. While there is clear-cut evidence of exfoliation and flattening in laser annealing, laser shock peening effectively presses the sample very hard to squeeze source-sink distance. Photo-acoustic measurements revealed that laser processing significantly improves thermal interfaces. It is believed that present findings on all-carbon robust thermal interfaces capable of fast removal of heat from hot-spots and withstanding thermal spikes/shocks in practical thermal chips would guide future research and expand the range of thermal management applications.

Introduction

Miniaturized nano electronic, photonic, and optoelectronic device components have been used in smart electronic gadgets in recent years. Advanced magnetic memory chips, for example, have nm-spaced circuit lines. Electrical energy dissipates and turns to heat when an electric current passes under the magnetic field created by nearby circuit components in nano electronic circuits. Nanomaterial-based energy storage devices under extreme loading face overheating problems. Several micromechanical components in advanced machines, such as micro gears, get extremely heated, and their structural fidelity is at risk. It is, therefore, urgent to find a solution for overheating of these technologically advanced nanochips/devices. Thermal interface materials (TIM) are employed as prompt thermal solutions. However, reliability issues of TIM restrict several materials to be used.[1] Ideal TIM, in general, needs to have high thermal conductivity, mechanical flexibility/robustness, and thermal stability. Moreover, for electrochemical devices, TIM should be robust against corrosion.

Carbon nanotubes (CNTs) are tubular quasi-1D nanomaterials having sp2-hybridized carbon atoms arranged in a honeycomb lattice. Owing to their structure and chemical bonding, CNTs are mechanically flexible and have high tensile strength and Young's modulus.[2,3] Carrier mobility better than silicon and electrical current carrying capacity better than copper makes CNTs a material with superior electronic performance.[4,5] Exciton formation and phonon-assisted relaxation make CNTs a photoluminescent material.[6] CNTs in general and vertical CNT arrays or CNT forests (CNTF) have been demonstrated to have good thermal conductivity,[7–11] due to which they show great promise as thermal interface materials.[12–16] However, mechanical shocks can disintegrate the bundle of CNTs in CNTF, thermal shocks can chemically degrade it by oxidation, and there is a danger of integrity when they are chemically treated. Such potential (physical and chemical) instabilities upon external stimuli (which are quite common from a practical applications point of view) restrict CNTF from fulfilling their great promise. Decorating CNTF with graphitic petals[17] (GP) is one of the feasible approaches towards providing them with adequate physical and chemical robustness.

a Birck Nanotechnology Centre, Purdue University, West Lafayette, Indiana, 47907, USA. E-mail: Prashant.Kumar@newcastle.edu.au, gjcheng@purdue.edu; Tel: +61 421639160, +1 765 49-45436

b School of Industrial Engineering, Purdue University, West Lafayette, Indiana, 47907, USA

c Global Innovative Centre for Advanced Materials, School of Engineering, The University of Newcastle, NSW-2308, Australia

d School of Mechanical Engineering, Purdue University, West Lafayette, Indiana, 47907, USA

† Electronic supplementary information (ESI) available. See DOI: https://doi.org/10.1039/d3ma00134b

‡ Current address: Arozona State Universitu, School for Engineering of Matter, Transport and Energy, USA.

§ Current address: University of Texas Dallas, Department of Mechanical Engineering, USA.

¶ Current address: UCLA, Mechanical & Aerospace Engineering, USA.

Graphene would structurally integrate well with carbon nanotubes as both belong to the same sp[2] carbon family. Moreover, graphenes themselves are good thermal conductors[18,19] and therefore have been employed as thermal interface materials.[20,21] Graphitic petals can handle heat bursts easily, would effectively enhance heat conducting channels by lateral connection, and would act as a shield for any seepage of metal coating on the top, which otherwise can form a pin-hole connection and can defeat the purpose. As-grown GP/CNTF are, however, protruded upwards or slanted and are sharp-featured, and if that top surface can be flattened, then all-carbon hybrid material (GP/CNTF) would be eligible for thermal interface applications.

Lasers have earlier been used for the modification of CNTs as well as graphene. Depending on the laser pulse duration and laser fluence values, by direct laser exposure, one can achieve (a) mild impact, such as local atonic-scale defect creation/annihilation upon local heating, (b) medium impact, such as exfoliation of graphene layers[22] or even (c) heavy impact, such as unzipping of CNTs,[23,24] or fragmenting of graphene. Moreover, laser energy can be adequately converted into pressure shock if laser plasma is confined. Such pressure shock can be used for material manipulation and for device integration seamlessly.[25–34] Thus, lasers can deliver optical energy in a controlled manner that gives rise to a suitable set of conditions of temperature and pressure required for the physico-chemical modification of carbon based SP[2] hybridized species such as CNTs and graphene. We have, therefore, employed post-growth laser processing to flatten the top surface of CNTFs, GPs and GPs/CNTFs hybrid. Direct laser exposure (predominantly thermal effect) and laser shock peening (using pressure shock, which is caused by the confinement of laser ablation plasma) have been employed on these samples. We have carried out field emission scanning electron microscopy (FESEM) and atomic force microscopy (AFM) to monitor the morphological modifications and Raman spectroscopy to diagnose the chemical quality of the modified materials. Thermal interface resistances were measured on these samples by photo-acoustic (PA) technique at various He pressure in a sapphire cell.

Results and discussion

The CNTFs (vertically aligned ultrathin threads of 10–20 micrometer length and 1.5–5 nm in diameter) are very delicate and fragile. CNTF grown on silicon substrates, when exposed to a focused laser (see the schematic in Fig. 1(a)), gives rise to vertical alignment and clustering, and cluster size is observed to be laser fluence dependent. The FESEM images in Fig. 1(b) show the surface morphology of an unirradiated CNTF sample. Fig. 1(c), (d), and (e) are the FESEM scan on the laser-irradiated surfaces when the laser beam was exposed through quartz plate at 5Hz repetition rate carried out for 3 min at 0.1, 0.2, and 0.4 J cm^{-2} fluences, respectively. At 0.1 J cm^{-2}, clustering commences, and there is a huge distribution of cluster size from 1.5 μm to 2.5 μm in Fig. 1(c). Increasing the laser fluence
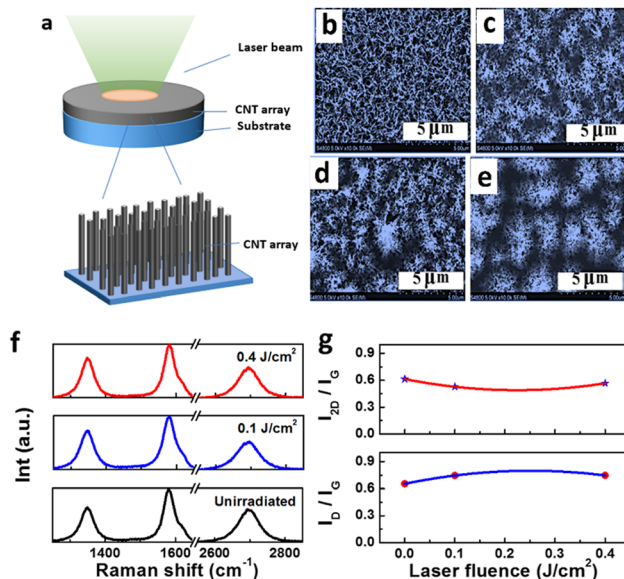

Fig. 1 (a) Schematic diagram for laser annealing of CNTF. FESEM images for CNTF for (b) untreated and laser annealed for 3 min at 5 Hz pulse rate at laser fluence value of (c) 0.1 J cm^{-2}, (d) 0.2 J cm^{-2}, and (e) 0.4 J cm^{-2}. (f) Raman spectra for untreated and laser annealed samples. Trends of I_D/I_G and I_{2D}/I_G with individual laser fluence used in isolated experiments.

to 0.2 J cm^{-2} under the same experimental conditions, some large size cluster starts forming and still have a large cluster size distribution, as can be witnessed from Fig. 1(d). When the sample was subjected to laser irradiation at 0.4 J cm^{-2}, large-sized clusters were formed with minimal variation in cluster size (see Fig. 1(e)).

Such cluster formation and vertical alignment can be attributed to the standing wave formed due to the incident laser beam interacting with the reflected laser beam from the metallic catalyst trilayers. Larger laser fluence would give rise to higher standing waves and consequently, more prominent vertical alignments. The standing wave formation will be limited to low laser power. However, at high laser power, laser-induced photo-thermal effect and quartz contact area will be influential. Fig. 1(f) shows the Raman spectra for unirradiated CNTF samples and those irradiated for 3 min and a pulse rate of 5 Hz at a laser fluence of 0.1 J cm^{-2} and 0.4 J cm^{-2}. Fig. 1(g) shows I_D/I_G and I_{2D}/I_G ratios as a function of laser fluence used for processing for the duration of 3 min and at a pulse rate of 5 Hz. No considerable changes have been observed in I_D/I_G ratio before and after laser processing, which means that there is no significant defect generation in the laser processing till 0.4 J cm^{-2}. Upto 0.4 J cm^{-2}, we could observe drastic changes in CNTF morphologies. They, in fact, cluster at the tip (see Fig. 1(e)). FESEM imaging and Raman spectroscopy for CNTF laser annealed with 0.8 J cm^{-2} at 5 Hz for 3 min duration shows surface carbonization by laser annealing (Fig. S1, ESI†). Since Raman spectroscopy is highly surface sensitive, we could observe the signature of carbonized CNTF, where the 2D peak dampens heavily. Usually, chemical processing of CNTs yield defects, and in that context, laser processing
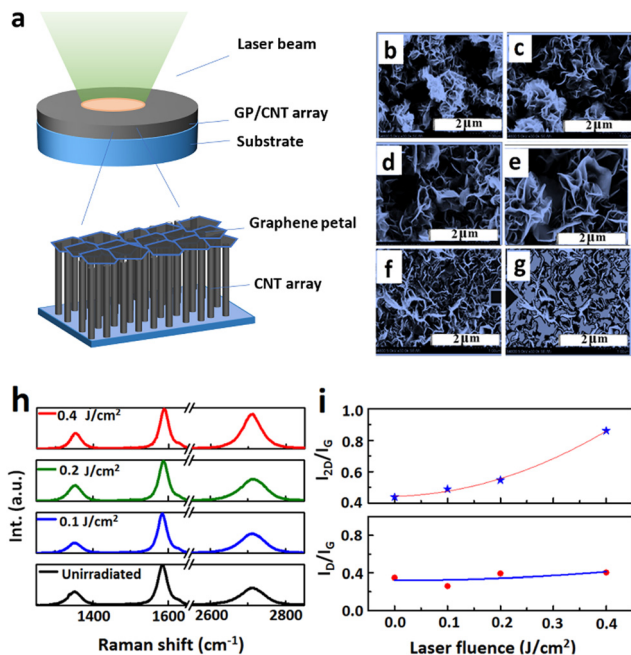
Fig. 2 (a) Schematic diagram of laser annealing of GP/CNTF. FESEM images of GP/CNTF surface for (b) untreated and laser annealed for 10 min at 5 Hz pulse rate at (c) 0.1 J cm^{-2}, (d) 0.2 J cm^{-2}, and at (e) 0.4 J cm^{-2}. FESEM of sample laser annealed at 0.4 J cm^{-2} for 10 min and at 10 Hz pulse rate (f). (g) Flattened area marked as a guide to eyes for easy recognition. (h) Raman spectra for untreated and laser annealed samples for 10 min and at 5 Hz. (i) trends of I_D/I_G and I_{2D}/I_G ratios with laser fluence used in isolated laser annealing experiments.

seems to be a relatively cleaner technique. In a quest to achieve a flattened surface on the top of graphitic petals coated on CNT forests, a prolonged annealing duration of 10 min and at the same pulse rate of 5 Hz was also attempted. Fig. 2(a) shows a schematic diagram showing the laser annealing of GP/CNTF samples. Fig. 2(b) shows the FESEM image of GP/CNTF without any laser treatment. Fig. 2(c), (d), and (e) show FESEM images of GP/CNTF samples laser processed at 0.1, 0.2, and 0.4 J cm^{-2}, respectively, each for 10 min duration of laser irradiation and at 5 Hz pulse rate. It seems that an increased laser pulse rate gives rise to enhanced exfoliation and flattening.

When the laser annealing duration is kept 10 min, but the pulse rate is doubled to 10 Hz, spectacular flattening is observed as shown in Fig. 2(f) and in false colour image Fig. 2(g), highlighting flattened area. As one can make out from Fig. 2(g), 40–50% of the total image area is flattened. Such flattening can be a combination of laser induced bending of petals and laser-induced exfoliation, which we will discuss later. Raman spectra of unirradiated sample and those irradiated at 0.1, 0.2, and 0.4 J cm^{-2} at 5 Hz pulse rate and for 10 min are shown in Fig. 2(h). I_{2D}/I_G and I_D/I_G ratios in Raman spectra in Fig. 2(h) are plotted in Fig. 2(i). One would expect two kinds of effects namely (a) exfoliation of graphitic petals and (b) flattening of vertical features. Local heating of defect sites at the edges of graphitic petals triggers exfoliation of petals and results in graphene layers coming off the petals. Flattening of vertical petals is a kind of physical effect brought in by laser,

which gives rise to radiation pressure as well as high local temperature. As can be observed from the ratio of the intensity of Raman peaks corresponding to 2D and G (*i.e.*, I_{2D}/I_G) and the ratio of Raman peak intensity for D and G peaks (*i.e.*, I_D/I_G), laser annealing does not induce many defects, and there is clear-cut evidence of laser-induced exfoliation as I_{2D}/I_G ratio increased significantly and in a systematic manner, while I_D/I_G remains almost constant. Such laser-induced quick processing of GP/CNTF hybrid nanoarchitectures yielding a significantly flattened surface, and importantly, bringing exfoliated graphene on the top will open the opportunity for such materials for potential applications. We have also carried out laser annealing at 0.8 J cm^{-2} for GP/CNTF. FESEM image (Fig. S2, ESI†) and AFM image (Fig. S3, ESI†) of this sample reveal surface flattening. However, laser damage is heavier than that for the sample with exposure to laser fluence of 0.4 J cm^{-2}.

Fig. 3(a) shows AFM images for unirradiated GP/CNTF samples and Fig. 3(b) and (c) show AFM images for the samples laser processed at 0.4 J cm^{-2} at pulse rates of 5 Hz and 10 Hz for 10 min, respectively. One observes that surface roughness of 300–500 nm for the unprocessed sample (see Fig. 3(a)) reduces to 30–50 nm when laser processed at 0.4 J cm^{-2} at 10 Hz for 10 min (see Fig. 3(c)). This proves a large-scale flattening of the top surfaces apart from the exfoliation effects. Bottom right corner shows line profiles in Fig. 3(a) and (c), respectively, which vividly showcase significant laser-induced flattening of the surface. Such flattening caused by KrF laser annealing with quartz cover ON is very exciting. Mostly, exfoliation of GNPs under UV transparent flat quartz slide contributes to the observed flattening.

Morphological changes brought by laser shock peening of CNTF and GP/CNTF samples are shown in Fig. 4(a) and (b), respectively. There is a clear-cut flattening, as shown in the top view in Fig. 4(a). However, the side view image on the laser shock peened CNTF sample shows heavy damage and the formation of amorphous carbon. In contrast, laser shock
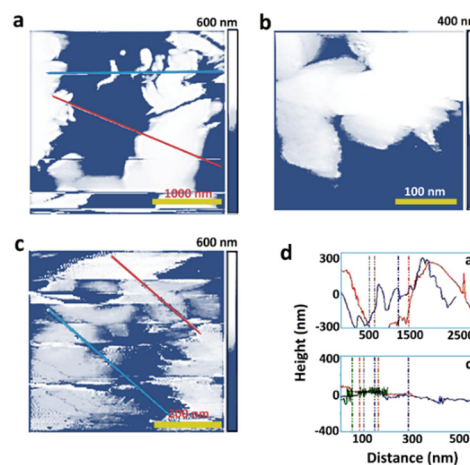

Fig. 3 AFM images for GP/CNTF samples for (a) untreated and for laser annealed for 10 min at 0.4 J cm^{-2} at (b) 5 Hz and (c) 10 Hz. Fourth panel in the bottom right shows a line profile along two lines drawn on (a) and (c).
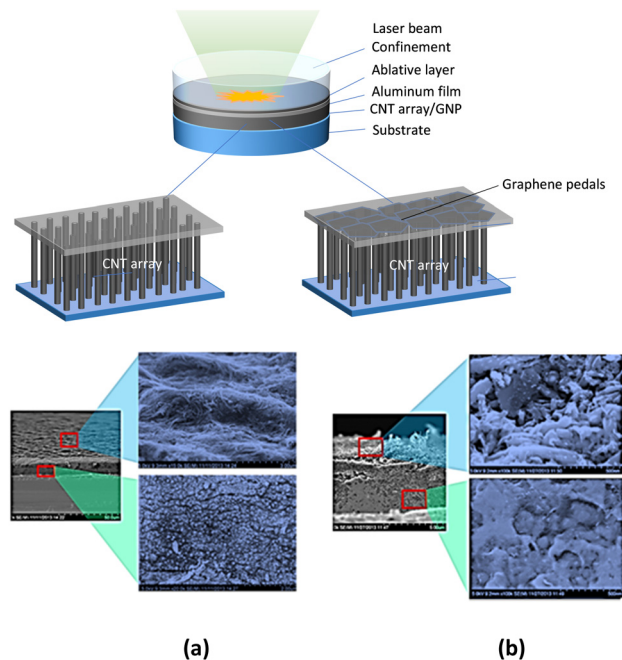
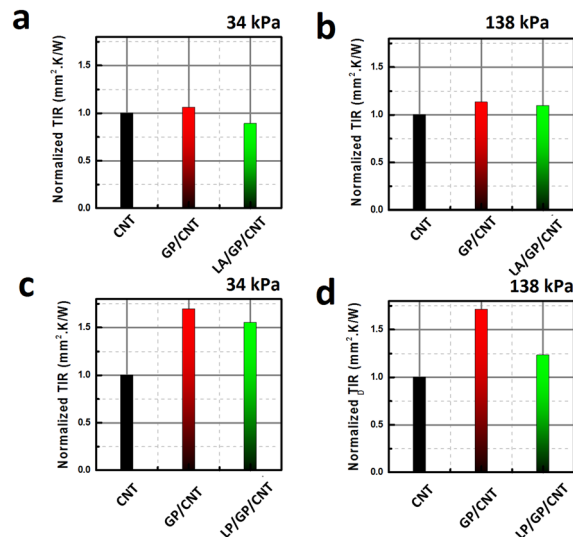Fig. 4 FESEM images of laser shock peened (a) CNTF and (b) GP/CNTF samples.

Fig. 5 Normalized TIR (normalized by that for carbon nanotubes) for untreated CNT and GP/CNT and laser annealed GP/CNT measured at (a) 34 kPa and (b) 138 kPa He pressure in PA cell. Normalized TIR for untreated CNT and GP/CNT and laser shock peened GP/CNT measured at (c) 34 kPa and (d) 138 kPa He pressure in PA cell.

peened GP/CNTF is not flattened as it was achieved in the case of CNTF. However, there is no structural damage as can be seen in the side-view image in Fig. 4(b) and this proves the robustness of GP coated CNTF samples.

Thermal interface resistances, as measured in photo-acoustic testing for CNTF, GP/CNTF, and laser annealed (LA) GP/CNTF samples at measurement He pressure of 34 and 138 kPa are shown in Fig. 5(a) and (b), respectively. Thermal interface resistances for laser shock peened GP/CNTF samples were also measured at 34 and 138 kPa He pressures and presented in Fig. 5(c) and (d), respectively.

The principle of photo-acoustic (PA) technique for thermal interface resistances is schematically shown in Fig. S5 (ESI†). It employs laser as a source to generate acoustic waves in a sample, and a microphone is used to detect these signals coming out of the sample situated on an automatically controlled heater stage. After having a vacuum in the sapphire PA cell, Helium gas is filled at a fixed pressure. It is concluded that irrespective of samples, graphitic petal coating increases thermal interface resistances, and laser processing (either laser annealing or laser shock peening) reduces the thermal interface resistance of GP/CNTF hybrid nanomaterials.

We have achieved laser annealing-induced vertical alignments and clustering of CNTF. Earlier, the femtosecond laser has been used to align CNT arrays orthogonally.[35] Such alignment and clustering would make the CNT arrays more robust towards mechanical and thermal shocks. Also, such a photo-induced assembly process would make them more responsive towards external triggers, as they would be laterally integrated and would behave as a unit within the cluster. We have achieved laser exfoliation and flattening of graphitic petals grown on vertical CNT arrays. Earlier, laser-induced

thinning[36] of multilayer graphene was reported. Laser-induced thinning is fundamentally an exfoliation process,[37–39] where the topmost graphene layer achieves sufficient energy to exceed the interaction with the layer beneath. Similarly, laser has earlier been used for micromachining of graphene, where it melts and joins the fragments.[40] Direct laser cutting of graphene has been reported earlier.[41] Also, the laser has been reported to conveniently shape graphene into desirable geometries exploiting the radiation pressure of laser beam.[42] Thus, we observe that in the literature, laser processing with adequate laser parameters can manoeuvre various physical modifications in graphene and carbon nanotubes.

Effective thermal interface resistance of TIM without any treatment can be written as:[42]

$$R_{TIM} = R_{C1} + \frac{BLT}{k_{CNT}} + R_{C2} + R_{C3}$$

where the bond line thickness of the TIM is BLT, and k_{CNT} is the thermal conductivity of CNTs. Thermal boundary resistance for Si/CNT, CNT/GNP, GNP/Cu interfaces are R_{C1}, R_{C2}, and R_{C3}, respectively (Fig. 6).

Upon laser annealing, a major improvement is expected at the GNP/Cu interface, as laser processing (annealing/shock peening) is a sort of surface dressing of GNPs, including their flattening and unzipping/exfoliation. Thus, R_{C3} will reduce substantially upon laser annealing. On the other hand, laser shock pressure treatment will primarily compress CNTs vertically with some local damage to petals, which effectively will reduce BLT. It should be noted that laser shock compression can induce huge compressive strain in CNTs, and in addition, some of CNTs can succumb under pressure shock loading and can undergo mechanical/structural failure and will bend/curl. In fact, direct laser exposure will not have any substantial effect
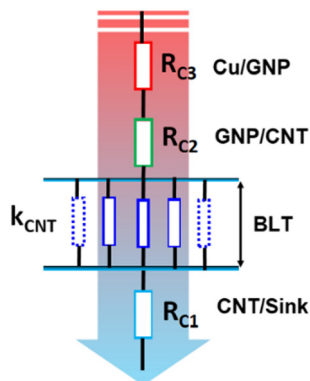
Fig. 6 Schematic diagram showing CNT/GNP based thermal interface materials.

on R_{C1} and R_{C2}. However, laser shock pressure will irreversibly press CNTFs, which will give rise to the buckling and interlinking of CNTs in the network.

According to Euler beam theory, below the threshold compression stress (σ_{crit}), elastic bending occurs, and CNTs strut turns unstable (buckling commences) just above the threshold compression stress (σ_{crit}).[43,44]

$$\sigma_{Th} = E_{CNT}(\pi r/L)^2$$

The Young's modulus of CNTs is E_{CNT}, and half wavelength of buckling along CNTs is L_{HW}. The threshold compression stress (σ_{crit}) for 20 nm diameter CNTs turns out to be $\sim$110 MPa. In particular, the defects in CNTs will reduce the threshold stress. In laser shock compression, the pressure is in the GPa range, and it is just 30 ns for a laser pulse. Short wavelength gives higher strain rate compression, which will lead to plastic (irreversible) deformation.

To capture the effect of high strain rate, the isotropic Johnson–Cook model is used.[45]

$$\sigma = \left(\sigma_y + K\varepsilon_p^{\,n}\right)\left[1 + C\ln\frac{\dot{\varepsilon}}{\dot{\varepsilon}_0}\right]\left[1 - \left\{\frac{T - T_0}{(T_{melt} - T_0)}\right\}^m\right]$$

σ_y is the initial room temperature yield stress (static), K and n are strain hardening consistency and strain hardening parameter, respectively, and C represents the strain rate sensitivity parameter. T_0 is room temperature, and T_{melt} is melting temperature. Plastic strain rate ($d\varepsilon/dt$) and reference strain rate ($d\varepsilon/dt$)$_0$ have been used in the strain rate sensitive term (second term). This equation can deal with strain rate sensitive elastic-plastic transition and strain hardening in CNTs. It should be noted that the strain rate in laser shock is above 10^6 s^{-1}.

Defects are predominantly responsible for local temperature rise in graphitic samples. Defect sites in CNTs and GNPs have dangling bonds and vacancies. When external laser power is applied to the system, these defects absorb the energy, and atomic vibrations increase, giving localized heat to the system. In general, high thermal conductivity materials, such as carbon nanotubes and graphene, are efficient in fast heat removal from the surface due to high thermal conductivity. In that context, defect sites will have a predominant role in heat accumulation.

For example, edges in graphitic petals and sharp tips in CNTs, which usually contain huge defect densities, would heat up more. For the case of a 5 Hz pulse rate, samples under our investigations are heated to an extreme temperature within the duration of 30 nanoseconds (which is the pulse width of the laser) and then would cool down within the next 200 milliseconds. For highly defective samples, the extreme temperature can even approach 3000 °C. CNTs and graphitic petals have good thermal conductivity,[46,47] which would help them to transmit heat energy created due to laser irradiation fast and thus homogenize the thermal profile throughout the volume. Since we used a quartz plate on top that allows the laser to go inside but does not allow the heat generated to go outside and it should be noted that we used silicon substrate and which is placed on an insulating plate while the laser irradiation experiment is carried out, heat would not escape easily. Also, the experiment was carried out in vacuum condition, which helps in retaining the heat in the system. For 3 min of laser irradiation at 5 Hz, this thermal cycle would repeat a total of 900 times, which would certainly have some accumulative effect on the final temperature. Similarly, 10 min of laser irradiation would give rise to 3000 and 6000 cycles for 5 Hz and 10 Hz pulse rate, respectively. Thus, even the slightest temperature rise per cycle (which is possible due to the thermal insulation of the system in our experiment), one would expect a considerable heat accumulation when a few thousands of such cycles is repeated. Such thermal processing in a pulsed manner would modify the system in a controlled manner, as one can precisely control the final temperature. Also, when the laser pulse rate is increased to 10 Hz, apart from the heat accumulation, there will be more effective pressure too, as highly energetic laser beams hit the material thousands of times. Radiation pressure would work as a kind of confinement to the heated material and would not allow it to spread vertically, and thus such interplay of temperature and pressure would result in the flattening of graphitic petals. An analogy can be drawn from flattening an iron bowl by hammering when it is red hot, in which case the combined effect of temperature and pressure can be witnessed. Laser processing of graphene ribbons has recently been used for direct lithography.[48] Laser can create local defects if it cuts graphene sheets locally and which would expose dangling bonds. If the laser-induced heating is sufficient to annihilate Stone-Wale's defects, one would achieve cleaner grains. Laser irradiation has earlier been reported to reduce lattice defects,[49] which possibly would enhance the stability of the systems as lattice defects give rise to instability.[50,51] Overall, some locations would witness defect rise and some would witness defect reduction, and therefore, in large scale measurements like Raman spectroscopy, which scans over 1 μm × 1 μm, measurement of defects would be averaged out over millions of defect centres. To our surprise, we have not seen any considerable rise in defect density due to laser processing.

The studies reported in this article represent initial attempts to exploit the tremendous potential of energetic laser beams for processing thermal interface materials consisting of graphene and carbon nanotubes and showcase improvement in

interfacial quality. Laser processing being a single-step, scalable, fast, and clean optical technique of surface modification, the prospect of such laser-based photophysical modification, which involves physico-chemical transformations in graphitic materials, seems encouraging due to the unprecedented freedom of selection of laser dressing parameters. We have demonstrated that adequate laser dressing parameters can result in various photophysical modifications that may be useful for specific applications. It is noteworthy that laser-induced modifications do not add up surplus chemical defects, as apparent from Raman results. We have observed that graphitic petals, when coated on the top of CNTF, invariably increase its thermal interface resistance and laser processing strategies adopted in our investigations (namely laser annealing and laser shock peening), both yield lowered thermal interface resistances. Other than the physical bending of outwardly protruding petals to make them flat, laser annealing causes the exfoliation of graphitic petals. Such flattening of petals helps minimize thermal loss at the surface. On the other hand, laser shock peening does not alter the surface as much as laser annealing does. However, laser shock peening presses the CNT forests sufficiently hard and in an infinitesimally short time. CNT forest could not resist the pressure shock and is forced to succumb. Under enormous peening pressure, not only the effective height of CNT forest is significantly reduced, CNTs curve too, and thereby, lateral joints develop midway. These physical effects, created by the plastic deformation of CNTs under peening pressure, reduce thermal interface resistance. Unevenly grown carbon nanotubes/graphitic petals have length non-uniformity, which is one of the serious concerns in TIM. Moreover, carbonaceous impurities at the tip of these grown CNTs or petals too hamper the prospects.[53]

In conclusion, it should be noted that GP/CNTF-based all-carbon thermal interface is very robust for extreme thermal spikes/shocks and apt for swift heat transfer from thermal hotspots, however, due to the roughness of the petal growth out-of-plane, interface quality is compromised. The present manuscript deals with the laser dressing/processing of the surface. New insight in the present report is the discovery of the use of laser annealing as well as laser shock peening of already grown CNTF, GP/CNTF samples to flatten them and achieve enhanced interface quality minimizing thermal interface resistance. CNTF vertically align themselves and form micro clusters upon laser annealing. Graphitic petals unfurl and get exfoliated upon laser annealing. Under a particular laser annealing condition, we have achieved a significant flattened area of up to 50% of the total area of the image on the surface of graphitic petal coated on CNTs. Surface roughness reduction by order of magnitude, as observed in AFM, supplements our findings based on FESEM. It is gratifying to note that laser annealing of graphitic materials is not adding surplus defects and hence proved to be a relatively clean technique as compared to contemporary chemical techniques. While laser shock peening of CNTF samples drops hints of significant structural damage, there is no damage in GP/CNTF, which proves that GP coating works as a shield against

mechanical stimuli. Laser processing (both laser annealing as well as laser shock peening) yields GP/CNTF samples with reduced thermal interfacial resistances. Findings of the present investigations are supposed to guide further research and widen the scope of electronic cooling applications of graphitic materials.

Materials and methods

A. Sample preparations

Carbon nanotubes were grown on silicon substrate using trilayer catalyst (Ti (30 nm), Al (10 nm), Fe (5 nm)). The details of the growth were reported elsewhere.[52] In summary, methane (flow rate of 10 sccm) as precursor gas in a hydrogen plasma (flow rate of 50 sccm) at a total pressure of 10 Torr was used for CNT growth in a microwave plasma chemical vapour deposition (MPCVD) system at substrate temperature of 800 °C for the duration of 10 min. For the growth of graphitic petals on the top of CNT arrays, precursor gas methane was used along with H_2 gas, and the growth time was 30 min and 20 min for samples GP/CNTF 1 and GP/CNTF 2, respectively, at a flow rate of 10 sccm for methane and that of 50 sccm for H_2 with the total pressure of 30 Torr. Carbon nanotubes were mostly multiwalled with a diameter in the range of 30–50 nm and an average length of ∼30 μm. Fig. S4 (ESI†) depicts the growth of materials.

B. Laser processing

Lambda Physik (Model LPX300) KrF excimer laser (λ = 248 nm, τ = 30 ns) was used for the laser processing of materials. Horizontal laser beams were bent perpendicularly to achieve a downward incident laser beam using a UV grade mirror and the beams were shaped into 1 cm × 1 cm square using a stainless-steel mask in the beam path. Laser irradiation experiment was carried out in a vacuum chamber having a top quartz cover, which is transparent to the laser. Laser parameters such as laser fluence, pulse rate, and irradiation time were varied to diagnose their impact on the resulting surface nanostructures. For each experiment, laser energy and beam area were measured. Three kinds of samples, (a) CNTF, (b) GP, and (c) GP/CNTF, were laser processed with the intention of surface modification to amend them for possible applications. Laser processing of samples soaked in conc. H_2SO_4 and then treated with $KMnO_4$ were also carried out to investigate whether such catalytic oxidation affects laser processing. Quartz plates were used as cover while laser exposure was carried out, and a thermally insulating plate was used underneath the sample in all the experiments. Quartz plate not only confines heat to the sample; it helps prevent laser evaporation of materials too. Silicon substrates were chosen for the experiment because materials investigated in this study would eventually have to be integrated into silicon technology for their application in thermal management for electronic devices. Laser energy was measured by a power meter from Molectron (Model ENERGY MAX500) that accurately measures laser energy with μJ precision. The meter reading is a statistical average of laser pulses

irradiated on its top photosensitive surface for 10 s. Calculation of laser fluence (energy/area) was carried out by dividing energy by 1 cm² exposure area. Apart from direct laser exposure (laser annealing), laser shock peening was also carried out, which uses laser shock pressure (GPa) achieved by confining laser ablation plasma when graphite coating was ablated. Aerosol graphite (Asbury Carbons, USA) coated on 4 μm thin Al foil (Lebow Company Inc., Bellevue, WA) was ablated by pulsed (10 ns) Q-switch Continuum Surelite Nd:YAG laser (second harmonic λ = 532 nm) with glass as confining medium. The laser beam was focused on a circle of 2 mm diameter. A computer controlled motorized XYZ stage was used for laser shock peening.

C. Microscopy and spectroscopy

Field emission scanning electron microscope (FESEM) (Hitachi S 4800 model) was used at an accelerating voltage of 5 keV for investigating morphological modification and atomic force microscope (AFM) (Veeco Instruments) in non-contact mode was used to explore the impact of laser processing on surface roughness. Chemical quality of materials was confirmed using a Raman spectrometer (Renishaw Inc.) with a green laser (λ = 532 nm) at 100× magnification.

Author contributions

PK, TSF, and GJC conceived the idea. PK made the samples and carried out KrF excimer laser irradiation and microscopy and spectroscopy. QN helped with laser shock peening and GX helped in AFM imaging. PK wrote the manuscript. PK and GJC revised it.

Data availability

Data is available upon request.

Conflicts of interest

Authors declare no conflict of interest.

Acknowledgements

References

1 J. Due and A. J. Robinson, *Appl. Therm. Eng.*, 2013, **50**, 455.
2 M.-F. Yu, O. Lourie, M. J. Dyer, K. Moloni, T. F. Kelly and R. S. Ruoff, *Science*, 2000, **287**, 637–640.
3 B. G. Demczyk, Y. M. Wang, J. Cumings, M. Hetman, W. Han, A. Zettl and R. O. Ritchie, *J. Mater. Sci. Eng. A*, 2002, **334**, 173–178.
4 X. Zhou, J.-Y. Park, S. Huang, J. Liu and P. McEuen, *Phys. Rev. Lett.*, 2005, **95**, 146805.
5 H. Dai, A. Javey, E. Pop, D. Mann, W. Kim and Y. Lu, *NANO: Brief Rep. Rev.*, 2006, **1**, 1–4.
6 K. Iakoubovskii, N. Minami, S. Kazaoui, T. Ueno, Y. Miyata, K. Yanagi, H. Kataura, S. Ohshima and T. Saito, *J. Phys. Chem. B*, 2006, **110**, 17420–17424.
7 Z. Han and A. Fina, *Prog. Polym. Sci.*, 2011, **36**, 914–944.
8 A. E. Aliev, M. H. Lima, E. M. Silverman and R. H. Baughman, *Nanotechnology*, 2010, **21**, 035709.
9 J. Hone, *Dekker Encycl. Nanosci. Nanotechnol.*, 2004, **120009128**, 603–610, DOI: 10.1081/E-ENN.
10 A. M. Nemilentsau and S. V. Rotkin, *ACS Nano*, 2012, **6**, 4298–4304.
11 I. Ivanov, A. Puretzky, G. Eres, H. Wang, Z. Pan, H. Cui, R. Jin, J. Howe and D. B. Geohegan, *Appl. Phys. Lett.*, 2006, **89**, 223110.
12 B. A. Cola, J. Xu, C. Cheng, X. Xu, H. Hu and T. S. Fisher, *J. Appl. Phys.*, 2007, **101**, 054313.
13 J. Xu and T. S. Fisher, *IEEE Trans. Compon. Packag. Technol.*, 2006, **29**, 261–267.
14 Y. Xu, Y. Zhang, E. Suhir and X. Wang, *J. Appl. Phys.*, 2006, **100**, 074302.
15 P. B. Amama, B. A. Cola, T. D. Sands, X. Xu and T. S. Fisher, *Nanotechnology*, 2007, **18**, 385303.
16 B. A. Cola, X. Xu, T. S. Fisher, M. A. Capano and P. B. Amama, *Nanoscale Microscale Thermophys. Eng.*, 2008, **12**, 228–237.
17 C. S. Rout, A. Kumar, T. S. Fisher, U. K. Gautam, Y. Bando and D. Golberg, *RSC Adv.*, 2012, **2**, 8250–8253.
18 A. A. Balandin, *Nat. Mater.*, 2011, **10**, 569–581.
19 A. A. Balandin, S. Ghosh, W. Bao, I. Calizo, D. Teweldebrhan, F. Miao and C. N. Lau, *Nano Lett.*, 2008, **8**, 902–907.
20 Q. Liang, X. Yao, W. Wang, Y. Liu and C. P. Wong, *ACS Nano*, 2011, **5**, 2392–2401.
21 K. M. F. Shahil and A. A. Balandin, *Nano Lett.*, 2012, **12**, 861–867.
22 P. Kumar, A. Dey, J. Roques, L. Assaud, S. Franger, P. Parida and V. Biju, *ACS Mater. Lett.*, 2022, **4**, 263.
23 P. Kumar, L. S. Panchakarla and C. N. R. Rao, *Nanoscale*, 2011, **3**, 2127.
24 P. Kumar, S. S. R. K. C. Yamijala and S. K. Pati, *J. Phys. Chem. C*, 2016, **120**, 16985.
25 S. R. Das, *et al.*, *ACS Nano*, 2015, **9**, 11121.
26 P. Kumar, J. Li, Q. Nian, Y. Hu and G. J. Cheng, *Nanoscale*, 2013, **5**, 6311.
27 Y. Hu, P. Kumar, R. Xu, K. Zhao and G. J. Cheng, *Nanoscale*, 2016, **8**, 172.
28 Y. Hu, P. Kumar, Y. Xuan, B. Deng, M. Qi and G. J. Cheng, *Adv. Opt. Mater.*, 2016, **4**, 1811.
29 Y. Hu, S. Lee, P. Kumar, Q. Nian, W. Wang, J. Irudayaraj and G. J. Cheng, *Nanoscale*, 2015, **7**, 19885.

30 S. Lee, P. Kumar, Y. Hu, G. J. Cheng and J. Irudayaraj, *Chem. Commun.*, 2015, **51**, 15494.

31 P. Kumar, *et al.*, *Nano Lett.*, 2018, **19**, 283.

32 J. Liu, Y. Hu, P. Kumar, X. Liu, J. M. K. Irudayaraj and G. J. Cheng, *Adv. Opt. Mater.*, 2021, **9**, 2001830.

33 M. Motlag, *et al.*, *Adv. Mater.*, 2019, **31**, 1900597.

34 P. Kumar and G. J. Cheng, *Laser and Photonic Systems: Design and Integration*, CRC Press, Taylor & Francis, 2014, vol 5, ISBN9780429101960.

35 R. D. Murphy, M. J. Abere, H. Zhang, H. Sun, B. Torralva, J. F. Mansfield, N. A. Kotov and S. M. Yalisove, *Appl. Phys. Lett.*, 2012, **101**, 203301.

36 G. H. Han, S. J. Chae, E. S. Kim, F. Gunes, I. H. Lee, S. W. Lee, S. Y. Lee, S. C. Lim, H. K. Jeong, M. S. Jeong and Y. H. Lee, *ACS Nano*, 2011, **5**, 263–268.

37 M. Qian, Y. S. Zhou, Y. Gao, J. B. Park, T. Feng, S. M. Huang, Z. Sun, L. Jiang and Y. F. Lu, *Appl. Phys. Lett.*, 2011, **98**, 173108.

38 U. Maitra, H. Matte, P. Kumar and C. N. R. Rao, *Chimia*, 2012, **66**, 941–948.

39 P. Kumar, *RSC Adv.*, 2013, **3**, 11987–12002.

40 W. Zhang, L. Li, Z. B. Wang, A. A. Pena, D. J. Whitehead, M. L. Zhong, Z. Lin and H. W. Zhu, *Appl. Phys. A: Mater. Sci. Process.*, 2012, **109**, 291–297.

41 G. Kalita, L. Qi, Y. Namba, K. Wakita and M. Umeno, *Mater. Lett.*, 2011, **65**, 1569–1572.

42 J. Li, T.-F. Chung, Y. P. Chen and G. J. Cheng, *Nano Lett.*, 2012, **12**, 4577–4583.

43 A. Nylander, *et al.*, *Energies*, 2019, **12**, 2080.

44 A. Cao, *et al.*, *Science*, 2005, **310**, 1307.

45 M. M. J. Treacy, T. W. Ebbesen and J. M. Gibson, *Nature*, 1996, **381**, 678.

46 G. Johnson and W. H. Cook, Proceedings of the 7th International Symposium on Ballistics. The Netherlands, 1983, 541–547.

47 A. Yu, P. Ramesh, M. E. Itkis, E. Bekyarova and R. C. Haddon, *J. Phys. Chem. Lett.*, 2007, **111**, 7565–7569.

48 P. Kim, L. Shi, A. Majumdar and P. L. McEuen, *Phys. Rev. Lett.*, 2001, **87**, 215502.

49 H. Tian, Y. Yang, D. Xie, T.-L. Ren, Y. Shu, H. Sun, C.-J. Zhou, X. Liu, L.-Q. Tao, J. Ge, C.-H. Zhang and Y. Zhang, *Phys. Chem. Chem. Phys.*, 2013, **15**, 6825–6830.

50 K. Qian, L. Zhou, J. Liu, J. Yang, H. Xu, M. Yu, A. Nouwens, J. Zou, M. J. Monteiro and C. Yu, *Sci. Rep.*, 2013, **3**, 1415.

51 M. H. Lu, Y. Q. Lai, G. N. Chen and Z. W. Cai, *Chem. Commun.*, 2011, **47**, 12807–12809.

52 H. Kawasaki, K. Nakai, R. Arakawa, E. K. Athanassiou, R. N. Grass and W. J. Stark, *Anal. Chem.*, 2012, **84**, 9268–9275.

53 L. Qiu, *et al.*, *Carbon*, 2017, **120**, 128–136.